

Separable-Potential Models of the Nucleon-Nucleon Interaction*

THOMAS R. MONGAN†

Lawrence Radiation Laboratory, University of California, Berkeley, California 94720

(Received 28 October 1968)

We present four different separable-potential models of the nucleon-nucleon interaction which fit both the low-energy data and the MacGregor-Arndt-Wright phase parameters for partial waves through $J=4$ in the energy range 0 to 400 MeV. The partial-wave scattering amplitudes resulting from our potentials have driving singularities at real negative values of the complex energy variable, and the appropriate amplitudes contain the deuteron pole and the singlet antibound-state pole at the correct energies. The present work extends and completes the results of an earlier paper.

INTRODUCTION

PREVIOUSLY,¹ we gave three separable potentials which fit the nucleon-nucleon scattering data. Now the Livermore group of MacGregor, Arndt, and Wright² has published the last of a series of papers on the determination of the nucleon-nucleon phase parameters. The appearance of these data has prompted us to extend and complete the work of Ref. 1.

We shall set forth four different separable-potential models of the nucleon-nucleon interaction. When separable potentials are inserted in the Lippmann-Schwinger integral equation for the off-energy-shell two-nucleon partial-wave scattering amplitude, the kernel of the equation becomes separable. Consequently the Lippmann-Schwinger equation can be solved algebraically. The resulting off-shell partial-wave amplitude is separable in the incident and outgoing relative momentum variables. Also, the off-shell amplitude is guaranteed to satisfy the five general nondynamical requirements laid down in Ref. 1, if the separable-potential form factors are properly chosen. That is, the off-shell partial-wave amplitudes resulting from our separable-potential models:

- (i) reduce to the correct on-shell amplitudes;
- (ii) satisfy off-energy-shell two-particle unitarity;
- (iii) have reasonable analyticity properties;
- (iv) are time-reversal invariant;
- (v) have the proper threshold behavior in both energy and momentum variables.

Because of their extreme simplicity, these separable-potential models should be useful in multiparticle scattering calculations. The fact that the off-shell behavior of these models is determined by the choice of the separable-potential form factors and the resulting amplitudes can be written as an off-shell factor multiplying the on-shell amplitude makes them useful in probing the off-shell behavior of two-body scattering amplitudes.

* Work supported in part by the U.S. Atomic Energy Commission.

† Present address: The MITRE Corporation, Westgate Research Park, McLean, Va. 22101.

¹ T. R. Mongan, Phys. Rev. **175**, 1260 (1968).

² M. H. MacGregor, R. A. Arndt, and R. M. Wright, Phys. Rev. **169**, 1128 (1968); and (to be published).

BASIC EQUATIONS

We consider models of the nucleon-nucleon interaction with a separable potential of the form

$$V_{l\nu}(p, p') = [i^{l(l-\nu)}] \cdot [g_l(p)g_\nu(p') - h_l(p)h_\nu(p')]. \quad (1)$$

This potential is to be inserted into the nonrelativistic two-particle partial-wave Lippmann-Schwinger equation, which for uncoupled waves is

$$T_l(p, p'; k^2) = V_l(p, p') + \frac{2\mu}{\hbar^2} \int_0^\infty \frac{dq q^2 V_l(p, q) T_l(q, p'; k^2)}{k^2 - q^2 + i\epsilon}, \quad (2)$$

where the c.m. kinetic energy $E = \hbar^2 k^2 / 2\mu$, and μ is the reduced mass of the two nucleons. For coupled waves, the Lippmann-Schwinger equation is

$$T_{l\nu}(p, p'; k^2) = V_{l\nu}(p, p') + \frac{2\mu}{\hbar^2} \sum_{j=J-1}^{J+1} \int_0^\infty \frac{dq q^2 V_{lj}(p, q) T_{j\nu}(q, p'; k^2)}{k^2 - q^2 + i\epsilon}.$$

The partial-wave T matrix obtained from the Lippmann-Schwinger equation is related to the partial-wave S matrix by

$$S_{l\nu}(k^2) = 1 - 2\pi i \rho_E T_{l\nu}(k^2),$$

where $\rho_E = \mu k / \hbar^2$. For uncoupled waves, the S matrix is given in terms of the phase shifts by $S_l(k^2) = \exp[2i\delta_l(k^2)]$ or

$$S_l(k^2) = 1 + 2i \exp[i\delta_l(k^2)] \sin\delta_l(k^2),$$

whence

$$\tan 2\delta_l(k^2) = -2\pi \rho_E \operatorname{Re} T_l(k^2) / [1 + 2\pi \rho_E \operatorname{Im} T_l(k^2)].$$

Alternatively, the T matrix can be expressed in terms of the phase shifts as

$$T_l(k^2) = -(1/\pi \rho_E) \exp[i\delta_l(k^2)] \sin\delta_l(k^2),$$

whence

$$\tan\delta_l(k^2) = \operatorname{Im} T_l(k^2) / \operatorname{Re} T_l(k^2).$$

For coupled waves, we use the Stapp³ parametrization

³ H. P. Stapp, T. J. Ypsilantis, and N. Metropolis, Phys. Rev. **105**, 302 (1957).

TABLE I. Case-I fits to nucleon-nucleon phase shifts in uncoupled partial waves. These partial waves are fitted by the separable potential

$$V_l(p, p') = g_l(p)g_l(p') - h_l(p)h_l(p'),$$

where the form factors are

$$g_l(p) = C_R p^l / (p^2 + a_R^2)^{(l+1)/2}, \quad h_l(p) = C_A p^l / (p^2 + a_A^2)^{(l+1)/2}.$$

The units of the attractive inverse range a_A and the repulsive inverse range a_R are inverse fermis (F^{-1} , $1F = 10^{-13}$ cm). The units of the attractive coupling strength C_A and the repulsive coupling strength C_R are $(\text{MeV } F)^{1/2}$. Dots indicate that a form factor is to be set equal to zero. ΣR^2 is the sum of the squares of the residuals:

$$\Sigma R^2 \equiv \sum_{i=1}^{28} [\delta_i^{\text{exp}}(E_i) - \delta_i^{\text{fit}}(E_i)]^2,$$

at the 28 data points in the range 0 to 400 MeV.

Partial wave	Repulsive potential parameters		Attractive potential parameters		ΣR^2
	a_R (F^{-1})	C_R ($\text{MeV } F)^{1/2}$	a_A (F^{-1})	C_A ($\text{MeV } F)^{1/2}$	
Singlet					
1S_0	2.331	52.45	1.855	41.36	469.3
1P_1	1.138	49.83	1.103	46.16	73.93
1D_2	1.418	4.817	5.253
1F_3	1.059	4.118	4.885
1G_4	1.076	2.300	0.139
Triplet					
3P_0	2.258	118.2	1.326	16.48	18.04
3P_1	0.697	3.498	2.322	18.89	0.091
3D_2	0.992	5.482	15.95
3F_3	0.837	2.347	0.120
3G_4	0.970	3.851	1.476

TABLE II. Case-II fits to nucleon-nucleon phase shifts in uncoupled partial waves. These partial waves are fitted by the separable potential

$$V_l(p, p') = g_l(p)g_l(p') - h_l(p)h_l(p'),$$

where the form factors are

$$g_l(p) = C_R p^l / (p^2 + a_R^2)^{(l+2)/2}, \quad h_l(p) = C_A p^l / (p^2 + a_A^2)^{(l+2)/2}.$$

The units of the attractive inverse range a_A and the repulsive inverse range a_R are inverse fermis (F^{-1} , $1F = 10^{-13}$ cm). The units of the attractive coupling strength C_A and the repulsive coupling strength C_R are $(\text{MeV}/F)^{1/2}$. Dots indicate that a form factor is to be set equal to zero. ΣR^2 is the sum of the squares of the residuals:

$$\Sigma R^2 = \sum_{i=1}^{28} [\delta_i^{\text{exp}}(E_i) - \delta_i^{\text{fit}}(E_i)]^2,$$

at the 28 data points in the range 0 to 400 MeV.

Partial wave	Repulsive potential parameters		Attractive potential parameters		ΣR^2
	a_R (F^{-1})	C_R ($\text{MeV}/F)^{1/2}$	a_A (F^{-1})	C_A ($\text{MeV}/F)^{1/2}$	
Singlet					
1S_0	6.157	302.0	1.786	27.33	456.3
1P_1	1.410	40.88	1.258	30.21	43.52
1D_2	1.944	21.09	8.577
1F_3	1.470	14.16	7.514
1G_4	1.425	8.502	0.257
Triplet					
3P_0	4.460	988.1	1.313	13.94	11.34
3P_1	2.178	45.63	56.06
3D_2	1.468	20.60	44.31
3F_3	1.213	7.247	0.766
3G_4	1.317	14.04	3.894

TABLE III. Case-III fits to nucleon-nucleon phase shifts in uncoupled partial waves. These partial waves are fitted by the separable potential

$$V_i(p, p') = g_i(p)g_i(p') - h_i(p)h_i(p'),$$

where the form factors are

$$g_i(p) = G_R \{ (1/\pi p^2) Q_i [1 + (\mu_R^2/2p^2)] \}^{1/2}, \quad h_i(p) = G_A \{ (1/\pi p^2) Q_i [1 + (\mu_A^2/2p^2)] \}^{1/2},$$

except in the partial waves 1S_0 , 3P_0 , and 1P_1 , where the repulsive form factor is $g_i^R(p) = \{ G_R p^2 / [p^2 + \frac{1}{2}(\mu_R^2)] \} \{ (1/\pi p^2) Q_i [1 + (\mu_R^2/2p^2)] \}^{1/2}$. $Q_i(x)$ is the Legendre function of the second kind. The units of the attractive inverse range μ_A and the repulsive inverse range μ_R are inverse fermis (F^{-1} , $1F = 10^{-13}$ cm). The units of the attractive coupling strength G_A and the repulsive coupling strength G_R are $(\text{MeV } F)^{1/2}$. Dots indicate that a form factor is to be set equal to zero. ΣR^2 is the sum of the squares of the residuals:

$$\Sigma R^2 = \sum_{i=1}^{28} [\delta_i^{\text{exp}}(E_i) - \delta_i^{\text{fit}}(E_i)]^2,$$

at the 28 data points in the range 0 to 400 MeV.

Partial wave	Repulsive potential parameters		Attractive potential parameters		ΣR^2
	μ_R (F^{-1})	G_R ($\text{MeV } F)^{1/2}$	μ_A (F^{-1})	G_A ($\text{MeV } F)^{1/2}$	
Singlet					
1S_0	2.225 ^a	20.84 ^a	1.300	10.00	1538.4
1P_1	0.644 ^a	26.53 ^a	1.256	31.53	44.22
1D_2	1.415	10.61	1.952
1F_3	0.933	12.06	2.304
1G_4	0.936	6.539	0.032
Triplet					
3P_0	1.799 ^a	291.5 ^a	1.475	26.65	158.9
3P_1	0.477	167.1	3.268	21.00	71.86
3D_2	5.663	108.5	1.057	15.40	11.16
3F_3	0.674	5.545	0.051
3G_4	0.799	9.513	0.050

^a Special repulsive form factor must be used.

TABLE IV. Case-IV fits to nucleon-nucleon phase shifts in uncoupled partial waves. These partial waves are fitted by the separable potential

$$V_i(p, p') = g_i(p)g_i(p') - h_i(p)h_i(p'),$$

where the form factors are

$$g_i(p) = C_R p^l / (p^2 + a_R^2)^{(l+1)}, \quad h_i(p) = C_A p^l / (p^2 + a_A^2)^{(l+1)}.$$

The units of the attractive inverse range a_A and the repulsive inverse range a_R are inverse fermis (F^{-1} , $1F = 10^{-13}$ cm). The units of the attractive coupling strength C_A and the repulsive coupling strength C_R are $[\text{MeV } F^{-(2l+1)}]^{1/2}$. Dots indicate that a form factor is to be set equal to zero. ΣR^2 is the sum of the square of the residuals:

$$\Sigma R^2 = \sum_{i=1}^{28} [\delta_i^{\text{exp}}(E_i) - \delta_i^{\text{fit}}(E_i)]^2,$$

at the 28 data points in the range 0 to 400 MeV.

Partial wave	Repulsive potential parameters		Attractive potential parameters		ΣR^2
	a_R (F^{-1})	C_R $[\text{MeV } F^{-(2l+1)}]^{1/2}$	a_A (F^{-1})	C_A $[\text{MeV } F^{-(2l+1)}]^{1/2}$	
Singlet					
1S_0	6.157	302.0	1.786	27.33	456.3
1P_1	1.967	121.6	1.566	49.73	25.31
1D_2	2.721	530.5	11.95
1F_3	2.341	1203.0	11.28
1G_4	2.387	3378.0	0.507
Triplet					
3P_0	5.000	1329.0	1.462	27.0	37.76
3P_1	2.661	200.3	63.85
3D_2	2.149	361.8	102.4
3F_3	2.010	428.3	2.332
3G_4	2.266	4881.0	9.605

TABLE V. Case-I fits to nucleon-nucleon phase parameters in coupled partial waves. These partial waves are fitted by the separable potential

$$V_{ll'}(p, p') = (i^{l+l'})[g_l(p)g_{l'}(p') - h_l(p)h_{l'}(p')],$$

where the form factors are

$$g_l(p) = C_l^R p^l / [p^2 + (a_l^R)^2]^{(l+1)/2}, \quad h_l(p) = C_l^A p^l / [p^2 + (a_l^A)^2]^{(l+1)/2}.$$

The units of the attractive inverse ranges a_{J+1}^A and a_{J-1}^A and the repulsive inverse ranges a_{J+1}^R and a_{J-1}^R are inverse fermis (F^{-1} , $1 F = 10^{-13}$ cm). The units of the attractive coupling strengths C_{J+1}^A and C_{J-1}^A and the repulsive coupling strengths C_{J+1}^R and C_{J-1}^R are $(\text{MeV } F)^{1/2}$. Dots indicate that a form factor is to be set equal to zero. ΣR^2 is the sum of the squares of the residuals:

$$\Sigma R^2 = \sum_{i=1}^{28} \{ [\delta_{J+1}^{\text{expt}}(E_i) - \delta_{J+1}^{\text{fit}}(E_i)]^2 + [\epsilon_J^{\text{expt}}(E_i) - \epsilon_J^{\text{fit}}(E_i)]^2 + [\delta_{J-1}^{\text{expt}}(E_i) - \delta_{J-1}^{\text{fit}}(E_i)]^2 \},$$

at the 28 data points in the range 0 to 400 MeV.

Coupled wave system	Parameters for $l=J+1$				Parameters for $l=J-1$				ΣR^2
	Repulsive parameters a_{J+1}^R (F^{-1})	C_{J+1}^R ($\text{MeV } F)^{1/2}$	Attractive parameters a_{J+1}^A (F^{-1})	C_{J+1}^A ($\text{MeV } F)^{1/2}$	Repulsive parameters a_{J-1}^R (F^{-1})	C_{J-1}^R ($\text{MeV } F)^{1/2}$	Attractive parameters a_{J-1}^A (F^{-1})	C_{J-1}^A ($\text{MeV } F)^{1/2}$	
$J=1$	0.848	20.38	0.744	10.82	3.990	22.98	0.982	9.804	1664.0
$J=2$	0.342	0.467	1.509	5.345	5.526
$J=3$	0.808	3.243	1.263	6.431	1.181	6.063	4.158
$J=4$	0.737	1.018	1.466	3.440	0.807

TABLE VI. Case-II fits to nucleon-nucleon phase parameters in coupled partial waves. These partial waves are fitted by the separable potential

$$V_{ll'}(p, p') = (i^{l+l'})[g_l(p)g_{l'}(p') - h_l(p)h_{l'}(p')],$$

where the form factors are

$$g_l(p) = C_l^R p^l / [p^2 + (a_l^R)^2]^{(l+2)/2}, \quad h_l(p) = C_l^A p^l / [p^2 + (a_l^A)^2]^{(l+2)/2}.$$

The units of the attractive inverse ranges a_{J+1}^R and a_{J-1}^R and the repulsive inverse ranges a_{J+1}^A and a_{J-1}^A are inverse fermis (F^{-1} , $1 F = 10^{-13}$ cm). The units of the attractive coupling strengths C_{J+1}^A and C_{J-1}^A and the repulsive coupling strengths C_{J+1}^R and C_{J-1}^R are $(\text{MeV}/F)^{1/2}$. Dots indicate that a form factor is to be set equal to zero. ΣR^2 is the sum of the squares of the residuals:

$$\Sigma R^2 = \sum_{i=1}^{28} \{ [\delta_{J+1}^{\text{expt}}(E_i) - \delta_{J+1}^{\text{fit}}(E_i)]^2 + [\epsilon_J^{\text{expt}}(E_i) - \epsilon_J^{\text{fit}}(E_i)]^2 + [\delta_{J-1}^{\text{expt}}(E_i) - \delta_{J-1}^{\text{fit}}(E_i)]^2 \},$$

at the 28 data points in the range 0 to 400 MeV.

Coupled wave system	Parameters for $l=J+1$				Parameters for $l=J-1$				ΣR^2
	Repulsive parameters a_{J+1}^R (F^{-1})	C_{J+1}^R ($\text{MeV}/F)^{1/2}$	Attractive parameters a_{J+1}^A (F^{-1})	C_{J+1}^A ($\text{MeV}/F)^{1/2}$	Repulsive parameters a_{J-1}^R (F^{-1})	C_{J-1}^R ($\text{MeV}/F)^{1/2}$	Attractive parameters a_{J-1}^A (F^{-1})	C_{J-1}^A ($\text{MeV}/F)^{1/2}$	
$J=1$	1.264	49.38	1.161	33.66	3.612	93.74	1.994	41.08	798.4
$J=2$	0.652	1.102	2.198	24.24	5.765
$J=3$	1.129	8.697	1.732	26.00	1.667	24.98	7.822
$J=4$	1.033	3.270	1.884	14.78	0.960

TABLE VII. Case-III fits to nucleon-nucleon phase parameters in coupled partial waves. These partial waves are fitted by the separable potential

$$V_{ll'}(p, p') = (i^{l+l'})[g_l(p)g_{l'}(p') - h_l(p)h_{l'}(p')],$$

where the form factors are

$$g_l(p) = G_l^R \{ (1/\pi p^2) Q_l[1 + ((\mu_l^R)^2/2p^2)] \}^{1/2}, \quad h_l(p) = G_l^A \{ (1/\pi p^2) Q_l[1 + ((\mu_l^A)^2/2p^2)] \}^{1/2},$$

where $Q_l(x)$ is the Legendre function of the second kind. In the $J=1$ system, the repulsive form factor for $J-1$ ($l=0$) is

$$g_l^R(p) = [G_l^R p^2 / (p^2 + \frac{1}{2}(\mu_l^R)^2)] \{ (1/\pi p^2) Q_l[1 + ((\mu_l^R)^2/2p^2)] \}^{1/2}.$$

The units of the attractive inverse ranges μ_{J+1}^A and μ_{J-1}^A and the repulsive inverse ranges μ_{J+1}^R and μ_{J-1}^R are inverse fermis (F^{-1} , $1 F = 10^{-13}$ cm). The units of the attractive coupling strength G_{J+1}^A and G_{J-1}^A and the repulsive coupling strengths G_{J+1}^R and G_{J-1}^R are $(\text{MeV } F)^{1/2}$. Dots indicate that a form factor is to be set equal to zero. ΣR^2 is the sum of the squares of the residuals:

$$\Sigma R^2 = \sum_{i=1}^{28} \{ [\delta_{J+1}^{\text{expt}}(E_i) - \delta_{J+1}^{\text{fit}}(E_i)]^2 + [\epsilon_J^{\text{expt}}(E_i) - \epsilon_J^{\text{fit}}(E_i)]^2 + [\delta_{J-1}^{\text{expt}}(E_i) - \delta_{J-1}^{\text{fit}}(E_i)]^2 \},$$

at the 28 data points in the range 0 to 400 MeV.

Coupled wave system	Parameters for $l=J+1$				Parameters for $l=J-1$				ΣR^2
	Repulsive parameters μ_{J+1}^R (F^{-1})	G_{J+1}^R ($\text{MeV } F)^{1/2}$	Attractive parameters μ_{J+1}^A (F^{-1})	G_{J+1}^A ($\text{MeV } F)^{1/2}$	Repulsive parameters μ_{J-1}^R (F^{-1})	G_{J-1}^R ($\text{MeV } F)^{1/2}$	Attractive parameters μ_{J-1}^A (F^{-1})	G_{J-1}^A ($\text{MeV } F)^{1/2}$	
$J=1$	0.592	77.49	0.511	18.10	3.249 ^a	71.99 ^a	1.458	13.94	2123.0
$J=2$	0.142	0.577	1.601	9.750	10.62
$J=3$	0.635	11.91	1.316	16.10	1.122	11.75	3.690
$J=4$	0.521	2.344	1.481	9.864	0.708

^a Special repulsive form factor must be used.

of the S matrix

$$S = \begin{pmatrix} \cos 2\epsilon e^{2i\delta_{J-1}} & i \sin 2\epsilon e^{i(\delta_{J-1} + \delta_{J+1})} \\ i \sin 2\epsilon e^{i(\delta_{J-1} + \delta_{J+1})} & \cos 2\epsilon e^{2i\delta_{J+1}} \end{pmatrix}.$$

Then, the coupled wave phase shifts and mixing parameters are given in terms of the T -matrix elements by

$$\begin{aligned} \tan 2\delta_{J-1} &= \frac{-2\pi \rho_E \operatorname{Re} T_{J-1, J-1}(k^2)}{1 + 2\pi \rho_E \operatorname{Im} T_{J-1, J-1}(k^2)}, \\ \tan 2\delta_{J+1} &= \frac{-2\pi \rho_E \operatorname{Re} T_{J+1, J+1}(k^2)}{1 + 2\pi \rho_E \operatorname{Im} T_{J+1, J+1}(k^2)}, \\ \sin 2\epsilon &= \frac{-2\pi \rho_E \operatorname{Re} T_{OD}(k^2)}{\cos(\delta_{J+1} + \delta_{J-1})}, \end{aligned}$$

where

$$T_{OD}(k^2) = T_{J-1, J+1}(k^2) = T_{J+1, J-1}(k^2).$$

The separable-potential formalism allows us to solve explicitly for the T matrix in the form $T_{ll'}(p, p'; k^2) = N_{ll'}(p, p'; k^2)/D_J(k^2)$, as well as the deuteron wave function, the deuteron D -state probability, and the deuteron quadrupole moment, in terms of the separable-potential form factors and certain integrals over these form factors. These results can be found in Ref. 1.

For $J=1$, the triplet scattering length a_t , the triplet effective range r_t , and the deuteron binding energy are related by

$$r_t = (2/k_D)[1 - (1/a_t k_D)], \quad (3)$$

where the deuteron binding energy is $E_D = \hbar^2 k_D^2/2\mu$. The position of the singlet antibound-state pole in the 1S_0 partial wave is related to the singlet effective range a_s and the singlet scattering length r_s by

$$k_V = \{1 - [1 - (2r_s/a_s)]^{1/2}\}/r_s, \quad (4)$$

where the pole occurs at the negative energy $E_V = -\hbar^2 k_V^2/2\mu$ on the second or unphysical sheet of the complex energy Riemann surface. The scattering lengths are given by

$$a_s = \lim_{k \rightarrow 0} (\pi\mu/\hbar^2) \operatorname{Re} T_0(k^2)$$

and

$$a_t = \lim_{k \rightarrow 0} (\pi\mu/\hbar) \operatorname{Re} T_{00}(k^2),$$

where $T_0(k^2)$ is the transition amplitude for 1S_0 scattering and $T_{00}(k^2)$ is the transition matrix element for $J=1, l=l'=0$.

We take for the nucleon mass M the average of the neutron and proton masses, so that $2\mu c^2 = Mc^2 = 938.903$ MeV and $\hbar c = 197.32$ MeV F. We take the deuteron binding energy $E_D = 2.22452$ MeV and the triplet scattering length $a_t = 5.396$ F, which yields a triplet

TABLE VIII. Case-IV fits to nucleon-nucleon phase parameters in coupled partial waves. These partial waves are fitted by the separable potential

$$V_{ll'}(p, p') = (p^{l'-1}) [g_l(p) g_{l'}(p') - h_l(p) h_{l'}(p')],$$

$$g_l(p) = C_{J+1}^R p^l / [p^2 + (a_{J+1}^R)^2]^{(l+1)}, \quad h_l(p) = C_{J-1}^R p^l / [p^2 + (a_{J-1}^R)^2]^{(l+1)},$$

where the form factors are $g_l(p) = C_{J+1}^R p^l / [p^2 + (a_{J+1}^R)^2]^{(l+1)}$ and $h_l(p) = C_{J-1}^R p^l / [p^2 + (a_{J-1}^R)^2]^{(l+1)}$. The units of the attractive inverse coupling strengths C_{J+1}^A and C_{J-1}^A and the repulsive inverse ranges a_{J+1}^R and a_{J-1}^R are inverse fermis ($F^{-1}, 1 F = 10^{-13}$ cm). The units of the attractive coupling strengths C_{J+1}^R and C_{J-1}^R and the repulsive coupling strengths a_{J+1}^A and a_{J-1}^A are $[\text{MeV } F^{-(\alpha+1)}]^{1/2}$. Dots indicate that a form factor is to be set equal to zero. ΣR^2 is the sum of the squares of the residuals:

$$\Sigma R^2 = \sum_{l=0}^{\infty} \{ [\delta_{J+1}^{\text{exp}}(E_i) - \delta_{J+1}^{\text{fit}}(E_i)]^2 + [\epsilon_{J+1}^{\text{exp}}(E_i)]^2 + [\delta_{J-1}^{\text{exp}}(E_i) - \delta_{J-1}^{\text{fit}}(E_i)]^2 \},$$

at the 28 data points in the range 0 to 400 MeV.

Coupled wave system	Parameters for $l=J+1$		Parameters for $l=J-1$		ΣR^2
	Repulsive parameters $a_{J+1}^R (F^{-1})$	Attractive parameters $C_{J+1}^A [MeV F^{-(\alpha+1)}]^{1/2}$	Repulsive parameters $a_{J-1}^R (F^{-1})$	Attractive parameters $C_{J-1}^A [MeV F^{-(\alpha+1)}]^{1/2}$	
$J=1$	1.738	477.4	3.472	85.53	1063.0
$J=2$	8.056
$J=3$	2.065	2151.0	2.331	465.1	18.17
$J=4$	1905.0
					1.353

TABLE IX. Case-I fits to nucleon-nucleon phase shifts in coupled waves, assuming $\epsilon_J=0$ and neglecting δ_{J+1} . These partial waves are fitted by the separable potential

$$V_i(p, p') = g_i(p)g_i(p') - h_i(p)h_i(p'),$$

where the form factors are

$$g_i(p) = C_R p^l / (p^2 + a_R^2)^{(l+1)/2}, \quad h_i(p) = C_A p^l / (p^2 + a_A^2)^{(l+1)/2}.$$

The units of the attractive inverse range a_A and the repulsive inverse range a_R are inverse fermis (F^{-1} , $1 F = 10^{-13}$ cm). The units of the attractive coupling strength C_A and the repulsive coupling strength C_R are $(\text{MeV } F)^{1/2}$. Dots indicate that a form factor is to be set equal to zero. ΣR^2 is the sum of the squares of the residuals:

$$\Sigma R^2 = \sum_{i=1}^{28} [\delta_i^{\text{exp}}(E_i) - \delta_i^{\text{fit}}(E_i)]^2,$$

at the 28 data points in the range 0 to 400 MeV.

Partial wave	Repulsive potential parameters		Attractive potential parameters		ΣR^2
	a_R (F^{-1})	C_R ($\text{MeV } F)^{1/2}$	a_A (F^{-1})	C_A ($\text{MeV } F)^{1/2}$	
3S_1	2.335	82.73	2.068	72.84	50.51
3P_2	1.509	5.349	0.406
3D_3	4.427	345.3	1.259	3.403	0.128
3F_4	1.530	3.663	0.068

TABLE X. Case-II fits to nucleon-nucleon phase shifts in coupled waves, assuming $\epsilon_J=0$ and neglecting δ_{J+1} . These partial waves are fitted by the separable potential

$$V_i(p, p') = g_i(p)g_i(p') - h_i(p)h_i(p'),$$

where the form factors are

$$g_i(p) = C_R p^l / (p^2 + a_R^2)^{(l+2)/2}, \quad h_i(p) = C_A p^l / (p^2 + a_A^2)^{(l+2)/2}.$$

The units of the attractive inverse range a_A and the repulsive inverse range a_R are inverse fermis (F^{-1} , $1 F = 10^{-13}$ cm). The units of the attractive coupling strength C_A and the repulsive coupling strength C_R are $(\text{MeV}/F)^{1/2}$. Dots indicate that a form factor is to be set equal to zero. ΣR^2 is the sum of the squares of the residuals:

$$\Sigma R^2 = \sum_{i=1}^{28} [\delta_i^{\text{exp}}(E_i) - \delta_i^{\text{fit}}(E_i)]^2,$$

for the 28 data in the range 0 to 400 MeV.

Partial wave	Repulsive potential parameters		Attractive potential parameters		ΣR^2
	a_R (F^{-1})	C_R ($\text{MeV}/F)^{1/2}$	a_A (F^{-1})	C_A ($\text{MeV}/F)^{1/2}$	
3S_1	4.540	127.4	1.908	35.02	60.63
3P_2	2.192	24.14	4.015
3D_3	6.558	493.8	1.451	7.716	0.189
3F_4	1.945	15.93	0.129

TABLE XI. Case-III fits to nucleon-nucleon phase shifts in coupled waves, assuming $\epsilon_J=0$ and neglecting δ_{J+1} . These partial waves are fitted by the separable potential

$$V_i(p, p') = g_i(p)g_i(p') - h_i(p)h_i(p'),$$

where the form factors are

$$g_i(p) = G_R \{ (1/\pi p^2) Q_i [1 + (\mu_R^2/2p^2)] \}^{1/2}, \quad h_i(p) = G_A \{ (1/\pi p^2) Q_i [1 + (\mu_A^2/2p^2)] \}^{1/2},$$

except in the fits to the partial wave 3S_1 , where the repulsive form factor is $g_i^R(p) = [G_R p^2 / (p^2 + \frac{1}{2}\mu_R^2)] \{ (1/\pi p^2) Q_i [1 + (\mu_R^2/2p^2)] \}^{1/2}$. $Q_i(x)$ is the Legendre function of the second kind. The units of the attractive inverse range μ_A and the repulsive inverse range μ_R are inverse fermis (F^{-1} , $1 F = 10^{-13}$ cm). The units of the attractive coupling strength G_A and the repulsive coupling strength G_R are $(\text{MeV } F)^{1/2}$. Dots indicate that a form factor is to be set equal to zero. ΣR^2 is the sum of the squares of the residuals:

$$\Sigma R^2 = \sum_{i=1}^{28} [\delta_i^{\text{exp}}(E_i) - \delta_i^{\text{fit}}(E_i)]^2,$$

at the 28 data points in the range 0 to 400 MeV.

Partial wave	Repulsive potential parameters		Attractive potential parameters		ΣR^2
	μ_R (F^{-1})	G_R ($\text{MeV } F)^{1/2}$	μ_A (F^{-1})	G_A ($\text{MeV } F)^{1/2}$	
3S_1	3.441 ^a	777.4 ^a	3.259	29.97	545.9
3P_2	1.600	9.764	2.622
3D_3	3.025	872.8	2.543	98.48	0.148
3F_4	1.581	10.83	0.010

^a Special repulsive form factor must be used.

TABLE XII. Case-IV fits to nucleon-nucleon phase shifts in coupled waves, assuming $\epsilon_J=0$ and neglecting δ_{J+1} . These partial waves are fitted by the separable potential

$$V_i(p, p') = g_i(p)g_i(p') - h_i(p)h_i(p'),$$

where the form factors are

$$g_i(p) = C_R p^l / (p^2 + a_R^2)^{(l+1)}, \quad h_i(p) = C_A p^l / (p^2 + a_A^2)^{(l+1)}.$$

The units of the attractive inverse range a_A and the repulsive inverse range a_R are inverse fermis (F^{-1} , $1 F = 10^{-13}$ cm). The units of the attractive coupling strength C_A and the repulsive coupling strength C_R are $[\text{MeV } F^{-(2l+1)}]^{1/2}$. Dots indicate that a form factor is to be set equal to zero. ΣR^2 is the sum of the squares of the residuals:

$$\Sigma R^2 = \sum_{i=1}^{28} [\delta_i^{\text{exp}}(E_i) - \delta_i^{\text{fit}}(E_i)]^2,$$

at the 28 data points in the range 0 to 400 MeV.

Partial wave	Repulsive potential parameters		Attractive potential parameters		ΣR^2
	a_R (F^{-1})	C_R $[\text{MeV } F^{-(2l+1)}]^{1/2}$	a_A (F^{-1})	C_A $[\text{MeV } F^{-(2l+1)}]^{1/2}$	
3S_1	4.540	127.4	1.908	35.02	60.63
3P_2	2.720	122.5	7.275
3D_3	2.489	307.8	2.253	248.0	0.775
3F_4	2.861	2115.0	0.237

effective range $r_s = 1.726$ F. We set the singlet anti-bound state at an energy $E_V = -0.0665$ MeV on the second sheet of the complex energy Riemann surface and we take the singlet scattering length $a_s = -23.678$ F, which yields a singlet effective range $r_s = 2.729$ F.

FORM FACTORS

The choice of a functional form for the repulsive form factor $g_i(p)$ and the attractive form factor $h_i(p)$ in Eq. (1) determines the off-shell behavior, the threshold behavior, and the analyticity properties of the off-shell scattering amplitudes as well as the asymptotic properties of the phase parameters. We have been particularly careful to choose functional forms which lead to an on-shell scattering amplitude

with driving singularities which lie *only* on the real negative axis in the complex energy plane. Thus our amplitudes have a singularity structure similar to that obtained from the fully relativistic theory of the nucleon-nucleon partial-wave amplitudes.

In case I, the form factors have the functional form $p^l / (p^2 + a^2)^{(l+1)/2}$, which has an asymptotic behavior like $1/p$ as $p \rightarrow \infty$, whereas in case II, the form factors are of the form $p^l / (p^2 + a^2)^{(l+2)/2}$, which goes as $1/p^2$ as $p \rightarrow \infty$. These cases correspond to choosing the first two members of the family of form-factor shapes discussed in Ref. 1. Of course, all our choices of separable-potential form factors behave like p^l at threshold, in order to produce the proper behavior of the phase parameters at threshold. Cases I and II in this paper

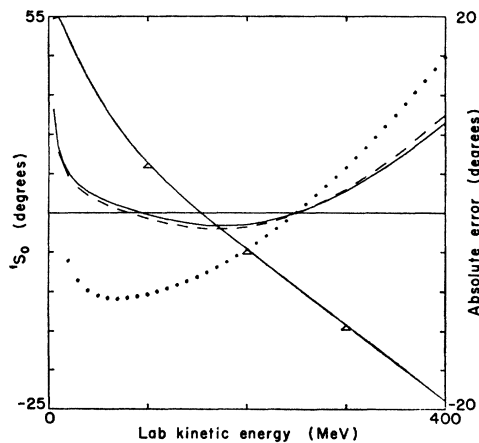


FIG. 1. Fits to the singlet phase shift 1S_0 . The curve marked Δ is the data value of the phase parameter in degrees and is read with the left-hand scale. The other curves are the absolute error (fitted value minus data value) in degrees of the various fits and are read with the right-hand scale. The dashed curve represents the case-I fit, the solid curve marks the case-II and case-IV fits, and the dotted curve indicates the case-III fit.

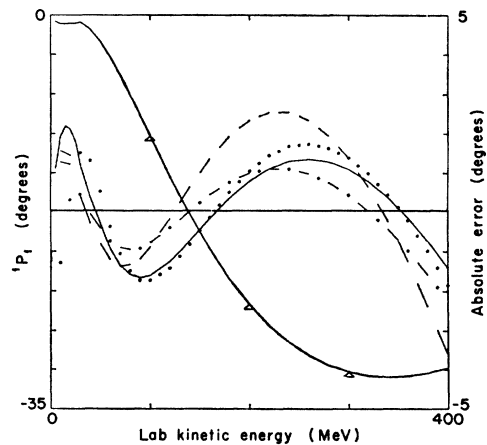


FIG. 2. Fits to the singlet phase shift 1P_1 . The curve marked Δ is the data value of the phase parameter in degrees and is read with the left-hand scale. The other curves are the absolute error (fitted value minus data value) and are read with the right-hand scale. The dashed curve represents the case-I fit, the solid curve marks the case-II fit, the dotted curve indicates the case-III fit, and the dot-dash curve denotes the case-IV fit.

TABLE XIII. Low-energy parameters.

1S_0 parameters				
	Singlet scattering length a_s (F)	Singlet effective range r_s (F)		
Experiment	-23.678	2.729		
Case I	-23.678	2.729		
Case II	-23.678	2.729		
Case III	-23.681	2.722		
Case IV	-23.678	2.729		
3S_1 parameters (coupling to 3D_1 neglected)				
	Triplet scattering length a_t (F)	Triplet effective range r_t (F)		
Experiment	5.396	1.726		
Case I	5.345	1.724		
Case II	5.396	1.726		
Case III	5.399	1.730		
Case IV	5.396	1.726		
$J=1$ parameters				
	Triplet scattering length a_t (F)	Triplet effective range r_t (F)	Deuteron quadrupole moment (F ²)	Deuteron D -state probability (%)
Experiment	5.396	1.726	0.278	...
Case I	5.654	2.041	0.277	0.7
Case II	5.384	1.710	0.276	1.1
Case III	5.565	1.936	0.278	0.5
Case IV	5.380	1.705	0.274	1.4

* All fits to the partial waves 1S_0 contain a singlet antibound-state pole at $E = -0.0665$ MeV on the second or unphysical sheet of the complex energy Riemann surface. All fits to the $J=1$ coupled wave system and to the 3S_1 partial wave neglecting the coupling to 3D_1 contain the deuteron pole at $E = -2.22452$ MeV on the physical sheet of the complex energy Riemann surface.

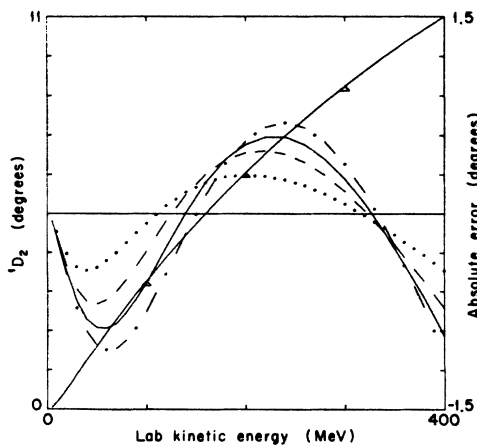


FIG. 3. Fits to the singlet phase shift 1D_2 . Description of curves is as for Fig. 2.

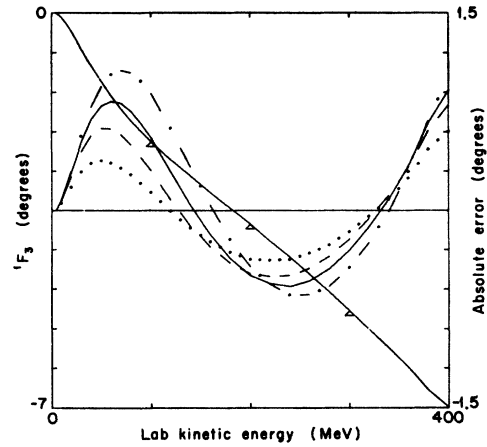


FIG. 4. Fits to the singlet phase shift 1F_3 . Description of curves is as for Fig. 2.

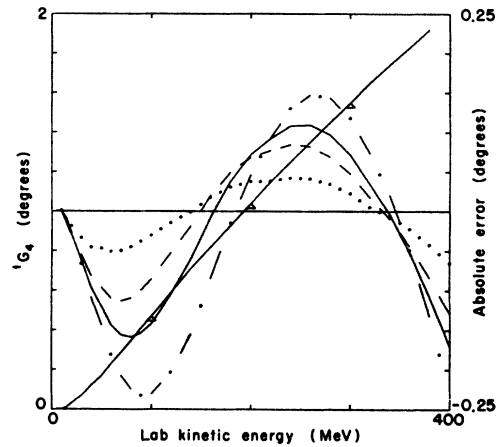


FIG. 5. Fits to the singlet phase shift 1G_4 . Description of curves is as for Fig. 2.

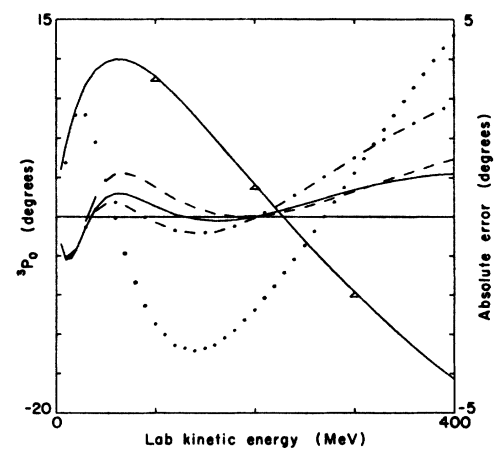


FIG. 6. Fits to the (uncoupled) triplet phase shift 3P_0 . Description of curves is as for Fig. 2.

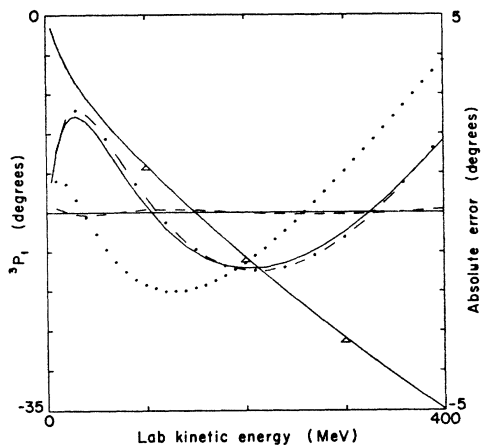


FIG. 7. Fits to the (uncoupled) triplet phase shift 3P_1 . Description of curves is as for Fig. 2.

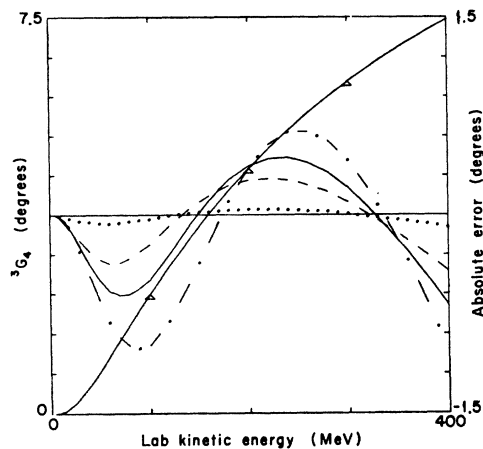


FIG. 10. Fits to the uncoupled triplet phase shift 3G_4 . Description of curves is as for Fig. 2.

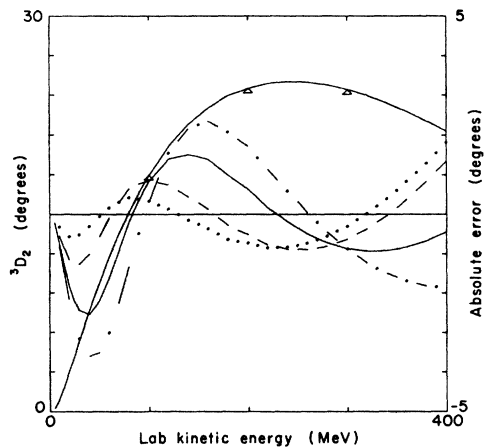


FIG. 8. Fits to the (uncoupled) triplet phase shift 3D_2 . Description of curves is as for Fig. 2.

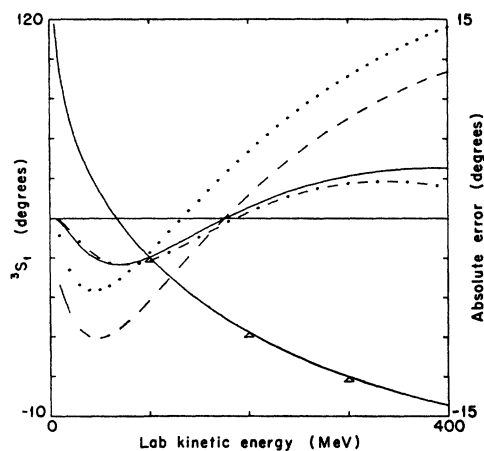


FIG. 11. Fits to the triplet phase shift 3S_1 ($J=1$ coupled waves). Description of curves is as for Fig. 2.

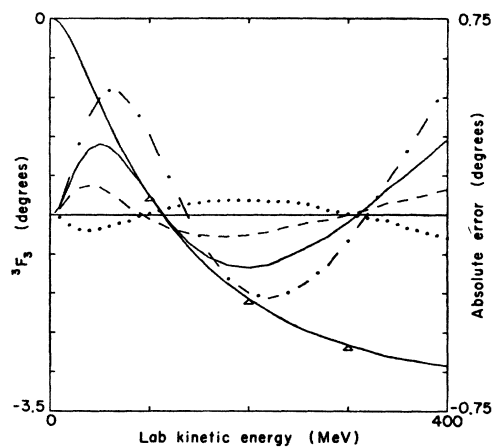


FIG. 9. Fits to the (uncoupled) triplet phase shift 3F_3 . Description of curves is as for Fig. 2.

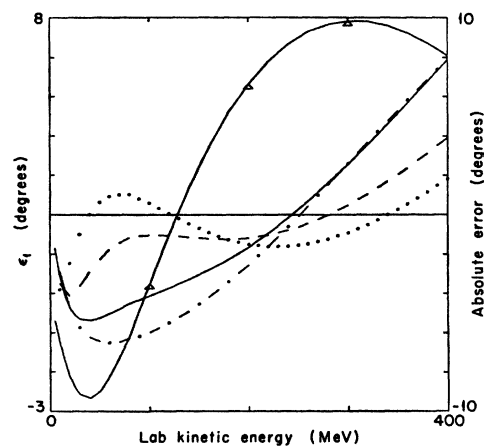


FIG. 12. Fits to the triplet mixing parameter ϵ_1 ($J=1$ coupled waves). Description of curves is as for Fig. 2.

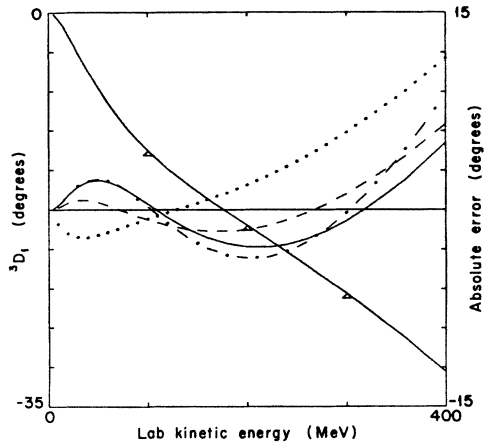


FIG. 13. Fits to the triplet phase shift 3D_1 ($J=1$ coupled waves). Description of curves is as for Fig. 2.

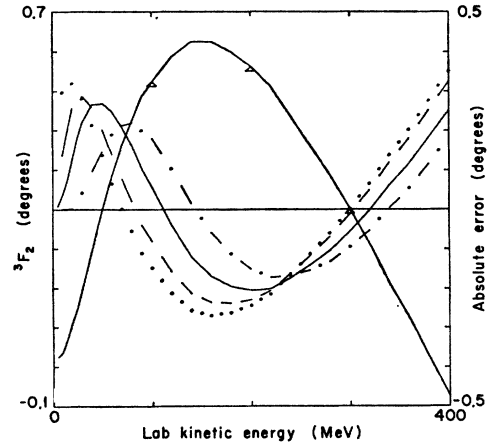


FIG. 16. Fits to the triplet phase shift 3F_2 ($J=2$ coupled waves). Description of curves is as for Fig. 2.

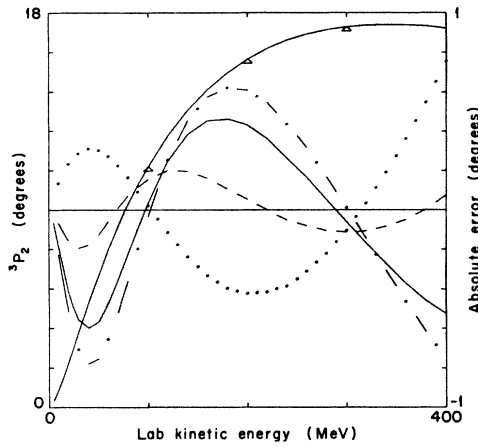


FIG. 14. Fits to the triplet phase shift 3P_2 ($J=2$ coupled waves). Description of curves is as for Fig. 2.

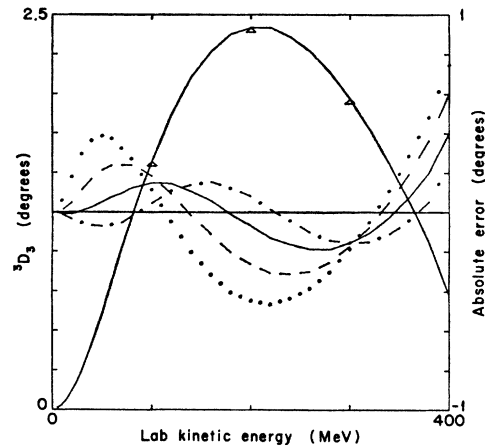


FIG. 17. Fits to the triplet phase shift 3D_3 ($J=3$ coupled waves). Description of curves is as for Fig. 2.

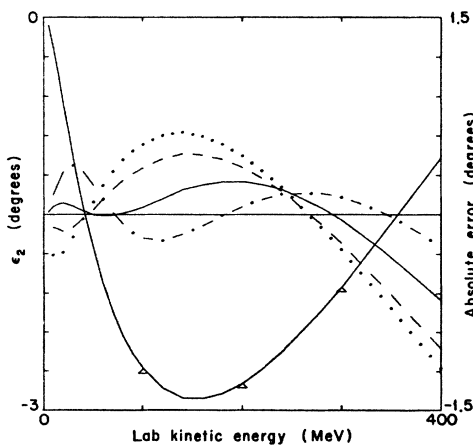


FIG. 15. Fits to the triplet mixing parameters ϵ_2 ($J=2$ coupled waves). Description of curves is as for Fig. 2.

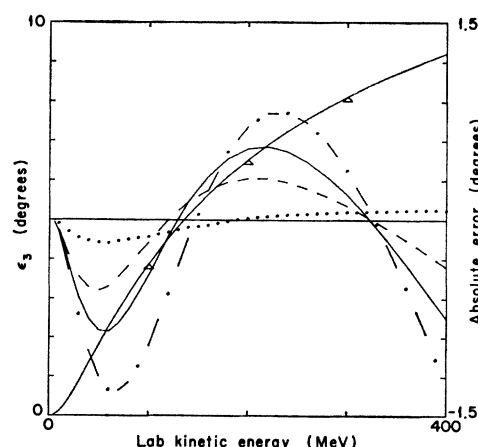


FIG. 18. Fits to the triplet mixing parameter ϵ_3 ($J=3$ coupled waves). Description of curves is as for Fig. 2.

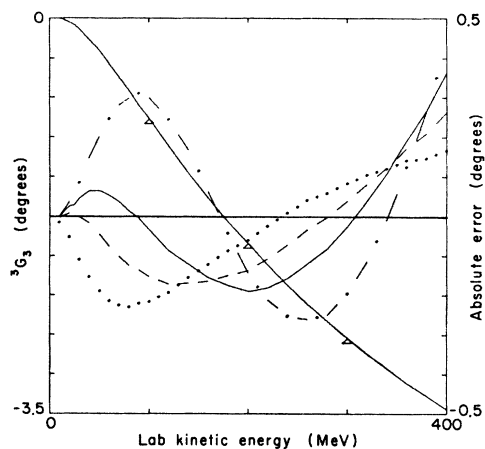


FIG. 19. Fits to the triplet phase shift 3G_3 ($J=3$ coupled waves). Description of curves is as for Fig. 2.

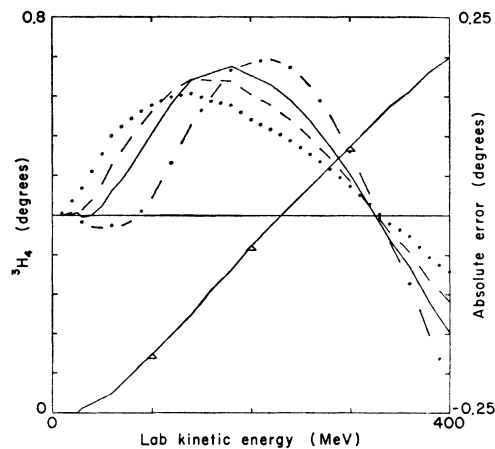


FIG. 22. Fits to the triplet phase shift 3H_4 ($J=4$ coupled waves). Description of curves is as for Fig. 2.

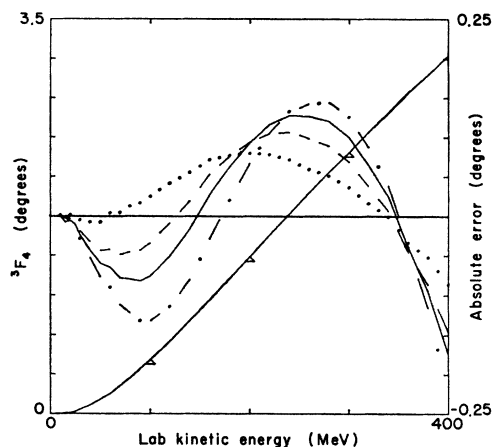


FIG. 20. Fits to the triplet phase shift 3F_4 ($J=4$ coupled waves). Description of curves is as for Fig. 2.

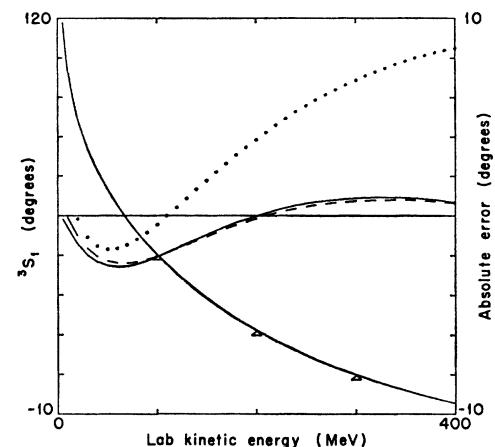


FIG. 23. Fits to the triplet phase shift 3S_1 (assuming $\epsilon_1=0$ and neglecting δ^3D_1). Description of curves is as for Fig. 1.

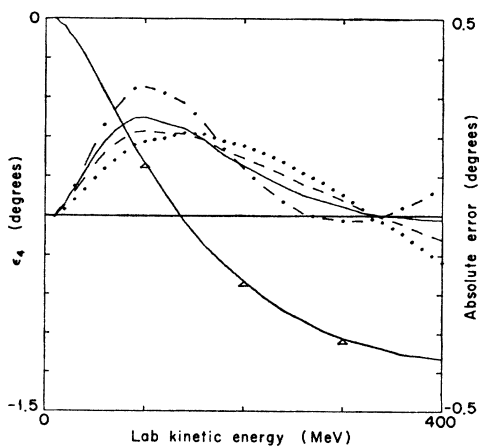


FIG. 21. Fits to the triplet mixing parameter ϵ_4 ($J=4$ coupled waves). Description of curves is as for Fig. 2.

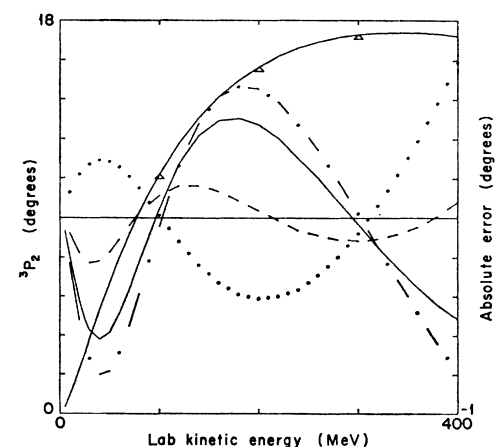


FIG. 24. Fits to the triplet phase shift 3P_2 (assuming $\epsilon_2=0$ and neglecting δ^3F_2). Description of curves is as for Fig. 2.

TABLE XIV. Maximum excursions of the error (fitted value minus data value) and the laboratory kinetic energies at which they occur.

Phase parameter	Maximum excursions of the error (deg)			
	Case I	Case II	Case III	Case IV
1S_0	{ 10.04 at 400 MeV -1.639 at 160 MeV	10.58 at 5 MeV -1.314 at 180 MeV	15.83 at 400 MeV -8.684 at 70 MeV	10.58 at 5 MeV -1.314 at 180 MeV
1P_1	{ 2.546 at 220 MeV -3.608 at 400 MeV	2.193 at 15 MeV -1.669 at 90 MeV	2.022 at 5 MeV -1.841 at 400 MeV	1.362 at 15 MeV -2.220 at 400 MeV
1D_2	{ 0.482 at 220 MeV -0.729 at 400 MeV	0.586 at 220 MeV -0.936 at 400 MeV	0.295 at 200 MeV -0.438 at 400 MeV	0.695 at 240 MeV -1.079 at 400 MeV
1F_3	{ 0.804 at 400 MeV -0.504 at 220 MeV	0.916 at 400 MeV -0.580 at 240 MeV	0.604 at 400 MeV -0.379 at 220 MeV	1.068 at 70 MeV -0.643 at 240 MeV
1G_4	{ 0.085 at 240 MeV -0.129 at 400 MeV	0.109 at 260 MeV -0.171 at 400 MeV	0.042 at 240 MeV -0.065 at 400 MeV	0.147 at 260 MeV -0.232 at 90 MeV
3P_0	{ 1.479 at 400 MeV -1.107 at 10 MeV	1.105 at 400 MeV -1.067 at 10 MeV	4.599 at 400 MeV -3.414 at 140 MeV	2.857 at 400 MeV -1.031 at 10 MeV
3P_1	{ 0.114 at 5 MeV -0.074 at 40 MeV	2.440 at 30 MeV -1.419 at 200 MeV	3.854 at 400 MeV -2.001 at 120 MeV	2.594 at 30 MeV -1.482 at 220 MeV
3D_2	{ 1.355 at 400 MeV -1.264 at 30 MeV	1.516 at 140 MeV -2.541 at 40 MeV	1.818 at 400 MeV -0.848 at 220 MeV	2.341 at 160 MeV -3.595 at 40 MeV
3F_3	{ 0.114 at 40 MeV -0.083 at 180 MeV	0.290 at 400 MeV -0.200 at 200 MeV	0.057 at 200 MeV -0.087 at 400 MeV	0.503 at 400 MeV -0.319 at 220 MeV
3G_4	{ 0.276 at 220 MeV -0.427 at 400 MeV	0.436 at 220 MeV -0.682 at 400 MeV	0.040 at 220 MeV -0.093 at 400 MeV	0.632 at 260 MeV -1.021 at 400 MeV
3S_1	{ 11.07 at 400 MeV -9.099 at 50 MeV	3.791 at 380 MeV -3.513 at 70 MeV	14.37 at 400 MeV -5.455 at 40 MeV	2.764 at 340 MeV -3.536 at 70 MeV
e_1	{ 3.904 at 400 MeV -4.132 at 20 MeV	7.891 at 400 MeV -5.371 at 40 MeV	1.803 at 400 MeV -3.364 at 5 MeV	7.877 at 400 MeV -6.505 at 60 MeV
3D_1	{ 6.501 at 400 MeV -1.647 at 160 MeV	5.127 at 400 MeV -2.838 at 220 MeV	11.54 at 400 MeV -2.100 at 40 MeV	8.723 at 400 MeV -3.682 at 200 MeV
3P_2	{ 0.201 at 120 MeV -0.194 at 30 MeV	0.462 at 180 MeV -0.599 at 40 MeV	0.754 at 400 MeV -0.422 at 200 MeV	0.620 at 180 MeV -0.778 at 40 MeV
e_2	{ 0.463 at 140 MeV -1.024 at 400 MeV	0.250 at 180 MeV -0.651 at 400 MeV	0.628 at 140 MeV -1.175 at 400 MeV	0.375 at 30 MeV 0.247 at 400 MeV
3F_2	{ 0.325 at 400 MeV -0.239 at 180 MeV	0.269 at 50 MeV -0.205 at 200 MeV	0.350 at 400 MeV -0.270 at 160 MeV	0.219 at 80 MeV -0.173 at 220 MeV

TABLE XIV (continued).

Phase parameter	Maximum excursions of the error (deg)			
	Case I	Case II	Case III	Case IV
3D_3	{ 0.602 at 400 MeV -0.313 at 240 MeV	{ 0.401 at 400 MeV -0.190 at 260 MeV	{ 0.746 at 400 MeV -0.465 at 220 MeV	{ 0.233 at 400 MeV -0.157 at 300 MeV
ϵ_3	{ 0.315 at 200 MeV -0.535 at 50 MeV	{ 0.556 at 200 MeV -0.852 at 60 MeV	{ 0.073 at 380 MeV -0.175 at 60 MeV	{ 0.813 at 240 MeV -1.306 at 70 MeV
3G_3	{ 0.267 at 400 MeV -0.172 at 120 MeV	{ 0.363 at 400 MeV -0.190 at 200 MeV	{ 0.167 at 400 MeV -0.231 at 80 MeV	{ 0.436 at 400 MeV -0.262 at 260 MeV
3F_4	{ 0.107 at 240 MeV -0.145 at 400 MeV	{ 0.128 at 240 MeV -0.174 at 400 MeV	{ 0.080 at 200 MeV -0.086 at 400 MeV	{ 0.144 at 280 MeV -0.220 at 400 MeV
ϵ_4	{ 0.215 at 100 MeV -0.061 at 400 MeV	{ 0.249 at 100 MeV -0.011 at 400 MeV	{ 0.210 at 140 MeV -0.117 at 400 MeV	{ 0.327 at 100 MeV -0.013 at 320 MeV
3H_4	{ 0.172 at 140 MeV -0.110 at 400 MeV	{ 0.188 at 180 MeV -0.149 at 400 MeV	{ 0.154 at 140 MeV -0.071 at 400 MeV	{ 0.197 at 220 MeV -0.210 at 400 MeV

differ from the corresponding cases in Ref. 1 in that we do not introduce any specially modified repulsive form factors.

For case III, we take form factors like

$$\{(1/p^2)Q_i[1+(\mu^2/2p^2)]\}^{1/2}$$

except in the partial waves 1S_0 , 3P_0 , 3S_1 , and 1P_1 , where the repulsive form factors have the form

$$[p^2/(p^2+\frac{1}{2}\mu^2)]\{(1/p^2)Q_i[1+(\mu^2/2p^2)]\}^{1/2}.$$

The Q_i functions are Legendre functions of the second kind. Both these forms have an asymptotic behavior like $[(\ln p^2)/p^2]^{1/2}$ as $p \rightarrow \infty$, and lead to on-shell amplitudes with cut singularities on the negative real energy axis. Separable-potential form factors like those

used in case III were first introduced by Mitra⁴ and we have used them because they promise the most realistic analyticity structure. This promise is belied by the fact that we must introduce special repulsive form factors, which have a pole at the start of the repulsive cut, in order to fit the phase shifts in the partial waves 1S_0 , 3P_0 , 3S_1 , and 1P_1 . In fact, the case-III fits are the least successful of our fits.

Finally, in case IV, we choose form factors of the form $p^l/(p^2+a^2)^{(l+1)}$, which behave as $1/p^{l+2}$ as $p \rightarrow \infty$. These form factors were chosen because they lead to off-shell amplitudes with the same asymptotic behavior in the momentum variables as the off-shell amplitude

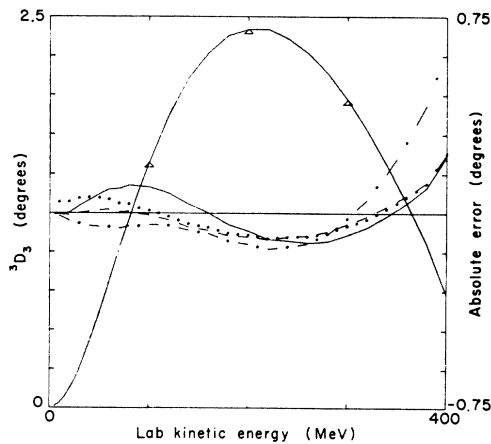


FIG. 25. Fits to the triplet phase shift 3D_3 (assuming $\epsilon_3=0$ and neglecting 3G_3). Description of curves is as for Fig. 2.

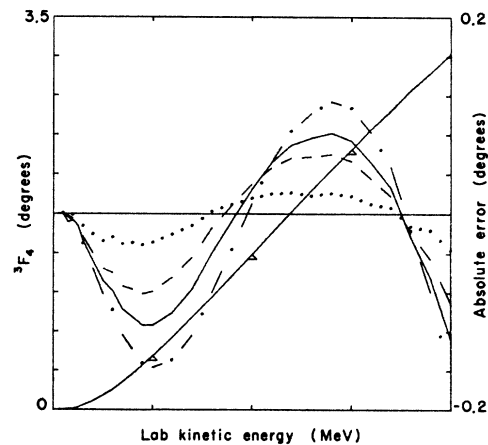


FIG. 26. Fits to the triplet phase shift 3F_4 (assuming $\epsilon_4=0$ and neglecting 3H_4). Description of curves is as for Fig. 2.

⁴ A. N. Mitra, Phys. Rev. **123**, 1892 (1961).

TABLE XV. Maximum excursions of the error (fitted value minus data value) and the laboratory kinetic energies at which they occur, for the phase shifts in coupled waves, assuming $\epsilon_J=0$ and neglecting δ_{J+1} .

Phase parameter	Maximum excursion of the error (deg)			
	Case I	Case II	Case III	Case IV
3S_1	{ 0.800 at 340 MeV -2.393 at 60 MeV	0.923 at 320 MeV -2.571 at 60 MeV	8.470 at 400 MeV -1.693 at 50 MeV	0.923 at 320 MeV -2.571 at 60 MeV
3P_2	{ 0.164 at 120 MeV -0.228 at 30 MeV	0.505 at 180 MeV -0.619 at 40 MeV	0.786 at 400 MeV -0.411 at 200 MeV	0.665 at 180 MeV -0.800 at 40 MeV
3D_3	{ 0.224 at 400 MeV -0.102 at 220 MeV	0.218 at 400 MeV -0.115 at 260 MeV	0.227 at 400 MeV -0.098 at 220 MeV	0.623 at 400 MeV -0.138 at 220 MeV
3F_4	{ 0.060 at 280 MeV -0.091 at 400 MeV	0.082 at 280 MeV -0.128 at 400 MeV	0.021 at 240 MeV -0.036 at 400 MeV	0.114 at 280 MeV -0.169 at 400 MeV

arising from a superposition of Yukawa potentials. This is easily seen by noting that a Yukawa potential in momentum space has the form $V_i(p, q) \sim (1/pq) \times Q_i[p^2 + q^2 + \mu^2/2pq]$, and the insertion of this potential into the Lippman-Schwinger equation (1) leads to an off-shell amplitude $T_i(p, q; k^2)$, which behaves like $1/p^{l+2}$ as $p \rightarrow \infty$ and like $1/q^{l+2}$ as $q \rightarrow \infty$.

In the $l=0$ partial wave, the case-II and case-IV form factors are identical. Case IV has the added advantage that all the integrals arising in the separable-potential formalism can, in principle, be done in closed form.

FIT TO THE NUCLEON-NUCLEON DATA

We have fitted our potentials to the MacGregor-Arndt-Wright (Livermore) nucleon-nucleon phase parameters for laboratory kinetic energy from 0 to 400 MeV for the partial waves through $J=4$. For each phase parameter we used the 28 data points, in the range 0 to 400 MeV laboratory kinetic energy E , provided by the energy-dependent phase parameter determination of MacGregor, Arndt, and Wright.

The fitting was accomplished on a CDC-6600 electronic computer at Lawrence Radiation Laboratory using LSQMIN, a least-squares minimization program developed by Eric Beals. The program LSQMIN searches for the values of the potential parameters that minimize the sum of the squares of the residuals at the 28 data

TABLE XVI. Grand total of the sum of the squares of the residuals for all uncoupled waves and coupled wave systems through $J=4$.

	Sum of squares of residuals
Case I	2263.7
Case II	1445.5
Case III	3966.9
Case IV	1811.9

points,

$$\sum R^2 = \sum_{i=1}^{28} [\delta_l^{\text{expt}}(E_i) - \delta_l^{\text{fit}}(E_i)]^2,$$

for uncoupled waves, and

$$\sum R^2 = \sum_{i=1}^{28} [\delta_{J-1}^{\text{expt}}(E_i) - \delta_{J-1}^{\text{fit}}(E_i)]^2 + \sum_{i=1}^{28} [\epsilon_J^{\text{expt}}(E_i) - \epsilon_J^{\text{fit}}(E_i)]^2 + \sum_{i=1}^{28} [\delta_{J+1}^{\text{expt}}(E_i) - \delta_{J+1}^{\text{fit}}(E_i)]^2,$$

for coupled waves.

The potential parameters that yield the best fit to the phase parameters are given in Tables I-VIII, where we have included the values of $\sum R^2$, since a comparison of these numbers for a single partial-wave or coupled-wave system gives an indication of the relative goodness of fit of the four cases.

We have displayed our fits to the phase parameters graphically in Figs. 1-22, where the curve marked Δ at 100-MeV intervals is the data value of the phase parameter in degrees and is read with the left-hand scale. The other curves are the absolute error (fitted value minus data value) in degrees of the various fits, and are read with the right-hand scale. The dashed curve represents the case-I fit, the solid curve marks the case-II fit, the dotted curve indicates the case-III fit, and the dot-dash curve denotes the case-IV fit.

For the convenience of those who would like to use these fits, neglecting partial waves with $l > l_{\text{max}}$, where l_{max} is 0, 1, 2, or 3, we have fitted the coupled waves 3S_1 , 3P_2 , 3D_3 , and 3F_4 , assuming $\epsilon_J=0$ and neglecting δ_{J+1} in each case. These results are presented in Tables IX-XII and Figs. 23-26.

We present the low-energy and bound-state parameters resulting from our potential models in Table XIII. In Table XIV we give the maximum positive and negative values of the errors and the energies at which they occur, for each fitting case in each partial wave. Similarly, Table XV lists the maximum error

excursions for the partial waves 3S_1 , 3P_2 , 3D_3 , and 3F_4 treated as uncoupled waves. Table XVI gives the grand total of the sum of the squares of the residuals in each fitting case. To form this sum, we sum the squares of the residuals in each uncoupled partial wave and each coupled wave system through $J=4$. The results show that case II gives the best over-all fit to the nucleon-nucleon scattering data.

In the partial wave 1S_0 we fit the phase shift and the three low-energy parameters: scattering length, virtual (antibound) state pole position, and effective range. These three parameters are related by Eq. (4), so that only two of them are independent. Consequently, we choose the scattering length $a_s = -23.678$ F and set the antibound-state pole at $E_V = -0.0665$ MeV on the second sheet of the complex energy Riemann surface, which implies a singlet effective range $r_s = 2.729$ F. The antibound-state pole on the second or unphysical sheet leads to a zero in the S matrix at the same energy on the physical sheet of the complex energy surface. In addition, the zero of the 1S_0 phase shift at 249.5 MeV implies that the N function in the separable-potential formula for the on-shell T matrix, $T_l(k^2) = N_l(k^2)/D_l(k^2)$, is zero at 249.5 MeV. To fit the 1S_0 partial wave, we use the conditions that the S matrix be zero at $E_V = -0.0665$ MeV and that the N function be zero at 249.5 MeV to determine the attractive and repulsive coupling strengths, and search for the values of the attractive and repulsive inverse ranges which give the best fit to the phase shift and scattering length. We then used Eq. (4) to determine the value of the effective range produced by the separable-potential models. Our 1S_0 scattering amplitudes are, therefore, *guaranteed* to contain the singlet antibound-state pole at the correct position on the unphysical sheet.

In the construction of our separable-potential models, we have made the tacit assumption of charge independence. When fitting the 1S_0 phase shifts, we biased the search procedure to ensure the correct values of a_s and r_s . However, the MacGregor-Arndt-Wright 1S_0 phase shifts are fitted to the proton-proton scattering length and effective range at low energy, and this explains the discrepancy between our fits and the phase shift data at low energies. We can fit the 1S_0 phase shifts quite closely, but then the absolute value of the scattering length becomes smaller. Note that the greatest error in our fits to the 1S_0 phase shift occurs at 400 meV, where the data value of the phase shift is -23.27° . However, the energy-independent determination of MacGregor, Arndt, and Wright gives a 1S_0 phase shift of -19.35° at 425 MeV, so our fits deviate from the energy-dependent data in the direction of the energy-independent value. In the absence of a charge-dependent determination of the 1S_0 phase shifts, we have presented what we feel is the best compromise.

When we fit the 3P_0 phase, which has a zero at 204 MeV, we use the condition that the N function of

the on-shell T matrix is zero at 204 MeV to determine the repulsive coupling strength. We then search for the values of the attractive coupling strength and the attractive and repulsive inverse ranges which produce the best fit to the phase shift data. However, in case III, we had to search with all four parameters free to obtain a reasonable fit.

If we consider the partial wave 3S_1 as if it were uncoupled, we wish the S matrix, and thus the T matrix, to have the deuteron pole at $E_D = -2.22452$ MeV on the physical sheet. This is accomplished by determining the attractive coupling strength from the condition that the D function in the separable potential expression for the on-shell T matrix have a zero at the deuteron pole position. Then we search for the values of the repulsive coupling strength and the attractive and repulsive inverse ranges which yield the best fit to the phase shift and scattering length, obtaining the effective range from Eq. (3).

When we consider the coupled waves with $J=1$, we again guarantee the correct binding energy for the deuteron by obtaining the attractive strength in $l=0$ from the condition that $D_{J-1}(k^2) = 0$ at $E_D = -2.22452$ MeV. Next we search for the values of the remaining seven potential parameters which give the best fit to the phase shifts, mixing parameter, scattering length, deuteron quadrupole moment, and D -state probability. We obtain the effective range from Eq. (3). Since the quadrupole moment of the deuteron is sensitive to the off-energy-shell behavior of the nucleon-nucleon interaction, we weight this quantity so that our searching routines are heavily biased in favor of those parameter sets which lead to a nearly correct quadrupole moment. We find that the resulting D -state probabilities are quite low, but since the available estimates of the D -state probability are imprecise and somewhat model-dependent, we do not feel that this is a serious drawback.

As an independent check on our work, our separable-potential models were put into computer programs which solve the Lippmann-Schwinger equations (1) and (2), with arbitrary well-behaved potentials, as complex matrix inversion problems. The latter programs were developed completely independently of the present work, and the agreement of the T matrices and phase parameters calculated from the two approaches constitutes the desired check of our work.

In conclusion, we suggest that whenever possible the form $T_{ll'}(p, p'; k^2) = F_{ll'}(p, p'; k^2) T_{ll}(k^2)$ be used in calculations when $k^2 > 0$, with $F_{ll'}(p, p'; k^2)$ obtained from the separable-potential models and $T_{ll}(k^2)$ expressed directly in terms of the experimental phase parameters. This separation has been discussed in Ref. 1, and it guarantees that the effect of on-shell two-body scattering is taken into account as accurately as possible in any calculation involving off-energy-shell two-body partial-wave scattering amplitudes, while retaining the advantage of separability in incident and outgoing momentum variables.